J Mater Sci (2011) 46:7696–7705
DOI 10.1007/s10853-011-5749-4

Microstructural investigations of XW-42 and M2 tool steels in semi-solid zones via direct partial remelting route

M. Z. Omar · A. Alfan · J. Syarif · H. V. Atkinson

Received: 19 April 2011 / Accepted: 25 June 2011 / Published online: 7 July 2011

Abstract A suitable microstructure for thixoforming consists of spheroidal grains in a liquid matrix. In order to achieve this, some processing routes have been established. In this study, microstructural evolution of XW-42 and AISI M2 steels via direct partial remelting from the as-annealed condition was examined. Both steels were found to possess certain types of carbides that dissolved when subjected to heating inside the semi-solid zones. The types of carbides were MC-M_6C for AISI M2 steel (fully dissolved between 1280 and 1300 °C) and M_7C_3 for XW-42 steel (fully dissolved between 1250 and 1270 °C). The dissolution of these grain boundary carbides during partial remelting helps with the grain spheroidisation and also with providing grain lubrication for the forming process through solid–liquid particle contact. In addition, solid–solid contacts were also observed (in 2D as well as 3D microstructural observation) and considered useful to provide structural integrity prior to forming. However, these contacts also must also be weak enough to be sheared easily. Compression test results for AISI M2 steel showed that thixotropic behaviour and complete mould filling were observed starting from 35 liquid percent. The same behaviour is also expected to occur for XW-42 steel due to its similarity in microstructural evolution with AISI M2 steel.

M. Z. Omar (✉) · A. Alfan · J. Syarif
Department of Mechanical and Materials Engineering, Faculty of Engineering and Built Environment, Universiti Kebangsaan Malaysia, 43600 Bangi, Selangor, Malaysia
e-mail: zaidi5886@gmail.com; zaidi@eng.ukm.my

H. V. Atkinson
Department of Engineering, University of Leicester, University Road, Leicester LEI 7RH, UK

Introduction

Thixoforming is a relatively new technology in which the metal is processed taking advantage of its thixotropic properties. In a thixotropic condition, an alloy experiences a fall in viscosity if it is sheared but it will thicken again if it is allowed to stand. This behaviour occurs due to the presence of a solid skeleton consisting of interconnected spheroidal grains in a liquid matrix that breaks during shearing [1]. The first experiment to demonstrate this thixotropic behaviour was conducted by Flemings and his co-workers in the early 1970s [2].

This new technology has enabled conceivable alternatives to conventional forming procedures such as casting or forging [3]. However, their use has until recently been restricted to alloys with relatively low melting points, namely magnesium- and aluminium-based alloys [4, 5] while for high melting point alloy (notably steel), there are still some obstacles that need to be tackled. Some of the obstacles are finding suitable tool materials [6–8] and achieving homogeneous heating of the billet [9]. Nevertheless, interest towards commercial use of steel for thixoforming is on the rise. For materials with high melting point such as steel, the advantage of thixoforming are low forging force compared to conventional forging processes, the possibility of forming components with complex and intricate shapes; reduction of steps in the forming process; less air entrapment and also less shrinkage porosity compared to conventionally casting processes [10]. Several steels such as HP9430 [10, 11], X210CrW12 [12–14], AISI 304 [15], 100Cr6 [16] and AISI M2 [17] have been investigated as candidate thixoforming materials. Recently, it was shown that the AISI M2 steel which contains high amount of carbon and carbide forming elements such as molybdenum, chromiun, vanadium and tungsten can be

subjected to a direct partial re-melting route, from its as-annealed condition, to obtain a thixoformable microstructure [17]. This was achieved without subjecting the material to any feedstock preparation process (such as cold or hot working) normally carried out to more established feedstock production routes such as recrystallisation and partial melting or strain-induced melt-activated. In this study, the semi-solid microstructures of XW-42 and AISI M2 steels prior to thixoforming are investigated, in particular to study the solid skeleton that supports the semi-solid structure prior to the thixoforming process. A 3-dimensional (3D) model of the semi-soild microstructure was constructed to analyse this skeleton. The microstructures were obtained when the steels were heated directly from their as-annealed conditions into their semi-solid zones through the direct partial re-melting route. The observation is focused at 20–50% liquid percent which is the usual working area for thixoforming processes [18].

Experimental procedure

Materials

The materials used in this work are XW-42 cold work tool steel and AISI M2 high speed steel. The XW-42 steel was supplied after soft annealing process, i.e. heating to 850 °C, followed by cooling at 10 °C/h to 650 °C and finally air cooling. The AISI M2 was supplied after hot forging at 1150 °C, followed by stress relieving at 650–750 °C for 4 h, then annealing at 860 °C for 8–10 h. Chemical compositions for the materials were acquired using Foundry-Master Spark Spectrometer for XW-42 steel and Inductive Couple Plasma Mass Spectroscopy (ICP-MS) combined with Leco CS 244 combustion type analyzer for AISI M2 steel.

JMatPro simulation

JMatPro (Java-based Material Properties) is a software package that was developed by Sente Software Ltd to augment the thermodynamic calculations by incorporating various theoretical material models and properties database that allow a quantitative calculation for the requisite materials property to be made within a larger software structure [19]. Here, the software is used to predict the reactions on solidification and liquid fractions of the investigated starting materials. The calculation is based on the application of an equilibrium solidification thermodynamic modelling route that has led to the ability to predict a number of critical thermophysical and physical properties for various alloys, including ferrous alloys. Such properties include the transformation of fraction of solid, enthalpy, specific heat, solidification shrinkage and various others.

Differential thermal analysis (DTA) measurement

DTA measurement was carried out to estimate solidus and liquidus temperatures as well as liquid fraction profile within the semi-solid zone and carbide stability zone of the two materials. The measurement was performed using a Netzsch simultaneous thermal analysis 409C equipment for the XW-42 steel with heating rate 5 °C/min and using a Perkin Elmer differential thermal analyser DTA7 for the AISI M2 steel with heating rate 20 °C/min. The sample was cut into small pieces with total weight of 50–100 mg with alumina as reference material.

Direct partial remelting experiment

The direct partial remelting experiment was performed using vertical, high temperature carbolite furnace. The material was cut into coupons with size of $5 \times 10 \times 12$ mm^3. Once the furnace has reached the set-up temperature, the coupon was lowered into the hottest position inside the furnace by using chromel wire. This will ensure a rapid heating of the coupon and it will normally arrived to the temperature in about 3 min. A K-type thermocouple placed inside a hole located on the 5×10 mm^2 surface of the coupon (5–6 mm deep) was used to monitor the temperature. The coupons were heated to temperatures that correspond to 20–50%, respectively, liquid percent with two different sets of holding times, 5 min for XW-42 steel and 4 min for AISI M2 steel. The heating was carried out in an argon atmosphere to reduce oxidation to the coupons. The selected temperatures for this direct partial remelting experiment were selected based on JMatPro simulation and also DTA test. After heating and holding at designated temperatures and holding times, the sample was quenched in brine solution.

Metallography and image analysis

The coupons from the direct partial remelting experiments were ground and polished to obtain clean and mirror-like surfaces. Subsequently, the coupons were etched using Villela reagent (1 g picric acid, 5 mL hydrochloric acid and 95 mL ethyl alcohol) to reveal their microstructures. Microstructural observation and analysis were conducted by using a BX-51 Olympus optical microscope as well as a Hitachi S3400N scanning electron microscope (SEM), equipped with energy dispersive spectroscopy (EDS). Average grain sizes were calculated by using mean lineal intercept method (after ASTM E112-96 standard).

To analyse the structure in more detail, a 3D model was constructed. Initially, the region of interest was marked by using microhardness tester. Then, series of planar sections were obtained by applying cyclic grinding and polishing to the sample which exhibited the clearest structure in 2D observation. The distance between those planar sections were also calculated. Then the model was constructed by using AutoCAD software. This process was first described by Niroumand and Xia [20].

Results and discussion

Starting materials

Table 1 shows chemical analysis result for XW-42 and AISI M2 steels. The result confirmed that the chemical composition of the alloys fell within the required standards [21, 22]. It should be noted that both steels possessed considerable amount of carbide forming elements such as chromium, vanadium and molybdenum.

Optical and SEM micrographs of as-received samples for XW-42 and AISI M2 steels are shown in Figs. 1 and 2.

Table 1 Chemical composition of XW-42 and AISI M2 steels (wt%)

Elements	Standard for AISI M2 [21]	Standard for XW-42 [22]	Test result for AISI M2	Test result for XW-42
C	0.8–0.5	1.4–1.6	0.9	1.5
Si	0.1–0.4	0.6 (max)	0.1	0.3
Mn	0.1–0.4	0.6 (max)	0.04	0.2
Cr	4–4.3	11–13	4.0	11.2
Ni	–	0.3 (max)	–	0.2
Mo	4.8–5.3	0.7–1.2	4.7	0.8
V	1.7–2.1	1.1 (max)	1.7	0.7
W	6–6.5	–	6.2	–

These arrays of carbides distributed homogeneously in bands parallel to the working direction. This structure is known to be found in as-annealed tool steel [21], thus confirming that annealing treatment was carried out as described by the material supplier. SEM–EDS analysis was conducted on the as-received samples for both steels (Table 2). The results showed that as-received XW-42 steel contained chromium rich carbides (both large and small types carbides), possibly an M_7C_3-type carbide (as this is also later shown by the JMatPro analysis). As for the as-received AISI M2 steel, SEM observation found whitish and greyish carbides. EDS examination found that the former was rich in tungsten and molybdenum (an M_6C-type carbide) while the latter were vanadium–tungsten–molybdenum rich MC-type carbide as already reported in Ref. [17].

Phase stability diagrams (Figs. 3 and 4) obtained from JMatPro simulation can be used alongside the SEM–EDS examination for the carbides found in both steels. The diagram for AISI M2 shows that at room temperature, the carbides consisted of M_6C, $M_{23}C_6$ and MC type carbides. However, $M_{23}C_6$ carbides were not detected during SEM–EDS observation. It was thought that the absence of $M_{23}C_6$ carbides can be explained by the fact that the steel was hot forged and annealed well above the carbide dissolution temperature at 828 °C (according to JMatPro simulation). In the same way, the soft annealing process at 850 °C can also explained about the absence of MC carbide in the as-received XW-42 steel (dissolution temperature at 740 °C).

Furthermore, the phase stability diagram can also be used to predict the type of carbides which dissolve in the semi-solid zone. Figure 3 shows that for AISI M2 steel, both M_6C and MC type carbides were found to dissolve inside the semi-solid zone. The MC carbides were found to dissolve at 1242 °C while the M_6C carbides dissolved later at 1275 °C. As for XW-42 steel, it can be observed that another type of carbide, M_7C_3, dissolved in the semi-solid zone (i.e. at 1251 °C). The dissolution of these carbides at

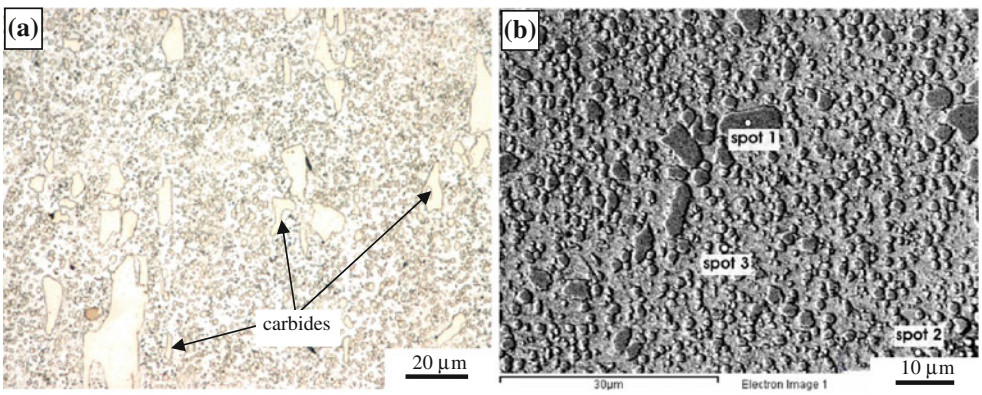

Fig. 1 Optical (**a**) and SEM (**b**) micrographs of as-received XW-42 steel

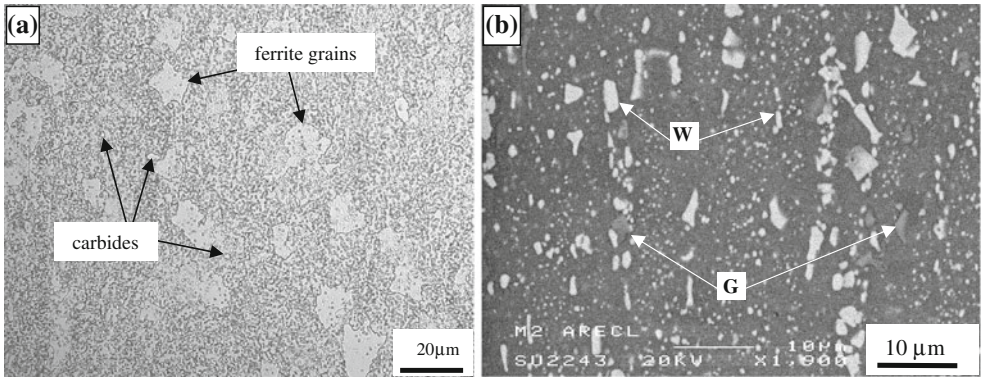

Fig. 2 Optical (**a**) and SEM (**b**) micrographs of as-received AISI M2 steel. *W* and *G* denote *whitish* and *greyish* carbides, respectively

Table 2 EDX analysis results of the carbides shown at Figs. 1 and 2

Material	Carbide	Weight					
		W	Mo	Cr	V	Fe	Co
AISI M2	Greyish carbides (MC)	19.4	18.4	4.9	28.1	28.9	0.4
		20.0	18.6	5.2	31.1	24.6	0.5
		19.2	17.5	4.8	23.9	34.9	–
	Whitish carbides (M_6C)	12.1	13.7	6.4	4.0	63.3	0.4
		13.1	14.1	6.7	3.8	61.7	0.4
		13.2	13.8	6.6	4.1	61.5	0.5
XW-42	Carbides (M_7C_3)	–	2.4	41.1	4.8	36.0	–
		–	2.3	39.4	4.3	38.7	–
		–	2.4	41.1	5.0	36.2	–

semi-solid zone causes the alloy to exhibit complex melting behaviour that is beneficial for thixoforming process. This will be further discussed in the subsequent section.

Liquid fraction profile

Liquid fraction profile (LFP) curves from JMatPro simulation and DTA test for XW-42 steel are shown in Fig. 5. It can be observed from these graphs that the start of solidus temperature was at around 1200–1220 °C while the liquidus fell between 1400 and 1415 °C. The total temperature interval for the semi-solid zone (between liquidus and solidus temperatures) was found to be between 180 and 215 °C. In comparison, Fig. 6 shows the LFP curves for AISI M2 steel which had liquidus line between 1235 and 1240 °C and solidus line between 1425 and 1458 °C. Thus, the semi-solid zone had a temperature interval of 185–223 °C. The two DTA and JMatPro curves in Fig. 5 are close together probably because the heating rate (DTA) is 5 °C/min and therefore relatively slow and closer to equilibrium. On the other hand, the DTA curve in Fig. 6 lags the prediction of JMatPro because probably there is no enough time for the liquid to form kinetically as the heating rate (DTA) is high, i.e. at 20 °C/min.

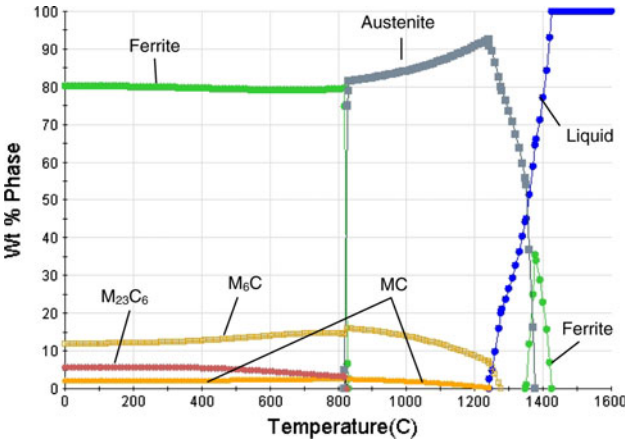

Fig. 3 Phase equilibrium diagram of AISI M2 steel obtained from JMatPro simulation

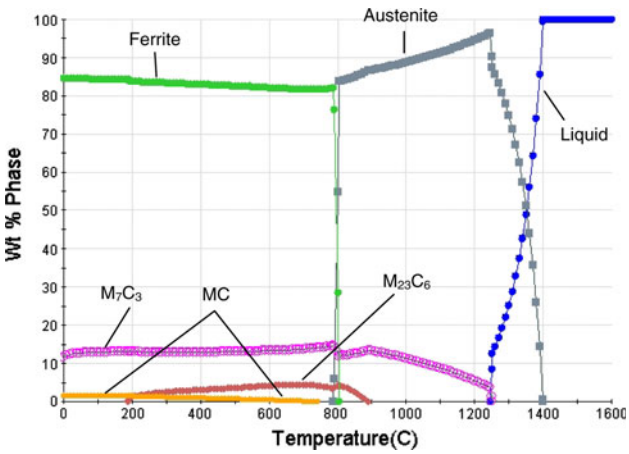

Fig. 4 Phase equilibrium diagram of XW-42 steel obtained from JMatPro simulation

As explained in the previous section, it is known that the dissolution of carbides at semi-solid zone affects its melting behaviour. Previous researchers [23, 24] have found that low temperature sensitivity had been observed for

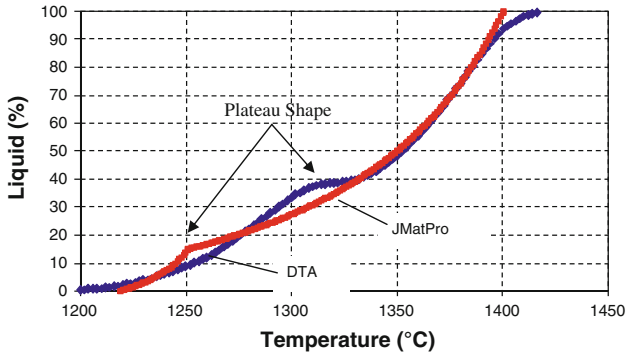

Fig. 5 Liquid fraction profile of XW-42 steel obtained from DTA (5 °C/min) and JMatPro simulation

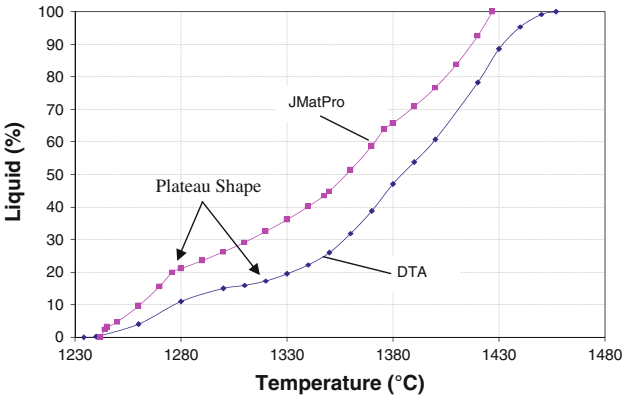

Fig. 6 Liquid fraction profile of AISI M2 Steel obtained from DTA (20 °C/min) and JMatPro simulation

steels with complex melting behaviour. The temperature sensitivity itself is defined as [25]:

$$S^* = \frac{\mathrm{d}x_\mathrm{L}}{\mathrm{d}T} \quad (1)$$

where S^* is the temperature sensitivity of an alloy, $\mathrm{d}x_\mathrm{L}$ is the selected liquid fraction interval of the alloy and $\mathrm{d}T$ is the temperature interval that is corresponded to the selected liquid fraction ($\mathrm{d}x_\mathrm{L}$). Hence, liquid percent in an alloy with low temperature sensitivity will be less sensitive to change in temperature.

The region with low temperature sensitivity was visible in LFP in the form of a near-horizontal plateau. As can be seen in Figs. 5 and 6, such plateau can be recognized in LFP for both steels. Differences in location for the plateaus between LFP obtained from JMatPro simulation and from DTA measurement are visible, especially for XW-42 steel. The differences occurs due the fact that the LFP from JMatPro software was generated using equilibrium condition whereas the one from DTA was experimentally obtained and in practice, the liquid takes time to form because of kinetic considerations. Hence, by considering both profiles, it was thought that the potential area in terms of temperature sensitivity lies between 1250 and 1340 °C for XW-42 steel. On the other hand, for AISI M2 steel, the near horizontal plateaus were located relatively at the same temperature interval for both DTA and JMatPro profiles, which is at around 1275–1320 °C. Thus, it could be said that in term of temperature sensitivity, these temperature intervals could be tempting for the thixoforming process. However, the corresponding microstructures of the materials and the liquid fractions at these intervals must also be taken into consideration.

Direct partial remelting

Microstructures of XW-42 and AISI M2 steels at the sub-solidus zone are shown in Fig. 7. For XW-42 steel, the selected sub-solidus temperature was at 1190 °C, while for AISI M2 steel, the temperature was 1220 °C. When comparing micrographs in Figs. 1 and 2 with those in Fig. 7, it is apparent that some of the carbides observed in the former have dissolved. The rest of the undissolved carbides are still contained in bands parallel to the working direction. Fine equiaxed grains also appeared in the background.

The microstructural evolution for both steels in the semi-solid zone is shown in Figs. 8 and 9 for XW-42 and

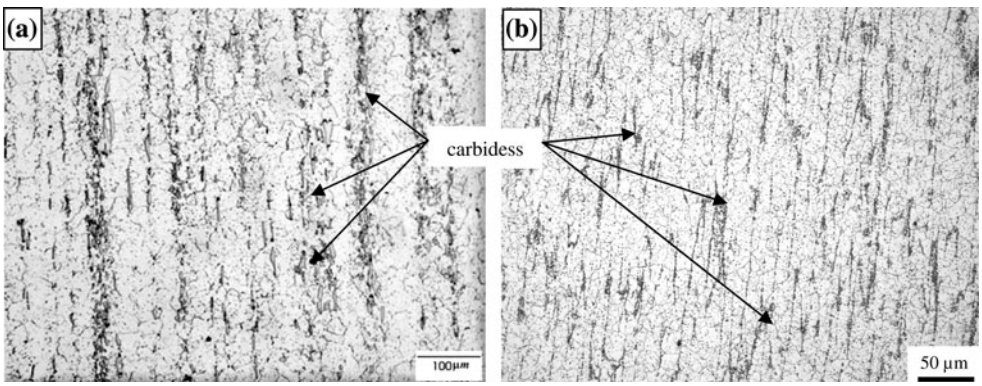

Fig. 7 Optical micrograph of **a** XW-42 and **b** AISI M2 steels after heating to the sub-solidus zone

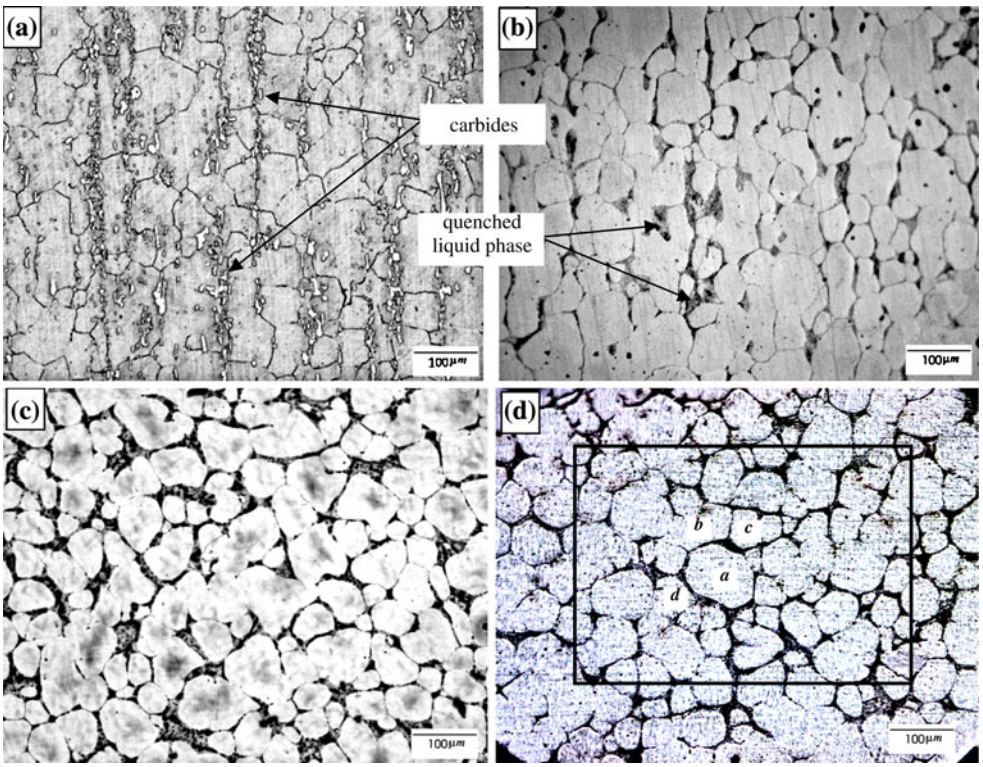

Fig. 8 Optical micrographs of XW-42 steel after being partial remelted at **a** 1250 °C, **b** 1270 °C, **c** 1300 °C and **d** 1340 °C with 5 min holding time. The *rectangle* in (**d**) indicates the region for 3D modelling

AISI M2 steels, respectively. Upon entering the semi-solid zone, more carbides are dissolved as compared to those in the sub-solidus condition. Consequently, equiaxed grains in the background start to appear clearly due to a decrease in the etchant preference effect towards the carbide. At the beginning of the semi-solid zone, the liquid and austenite phases coexisted with the carbides (Figs. 8a, 9a). Since no structure such as lamella structure or martensitic structure was observed at inner grain of austenite after quenching, it is thought that the austenite phase was stable at room temperature due to the high content of carbon and chromium for both steels (see Table 1) which shifted the eutectic transformation to longer time and lowered the martensite start temperature [13]. The carbide dissolution temperatures for both steels as obtained from partial remelting experiments were somewhat higher compared to those from JMatPro calculations mentioned earlier. For XW-42 steel, the observed carbide dissolution temperature for M_7C_3 type carbide was found to be in the range of 1250–1270 °C (see Fig. 8a, b), whereas for AISI M2 steel, the temperature range was between 1240 and 1280 °C (see Fig. 9a, b).

As can be seen in Fig. 8b, after the carbide dissolve completely at 1270 °C, the austenite grains are still seen in the equaixed shape for the XW-42 sample. Further heating to 1300 °C (Fig. 8c) and 1340 °C (Fig. 8d) show that the equiaxed grains were transformed into near-spheroidal grains. These temperatures correspond to 35 and 43 liquid percent, respectively according to liquid fraction profile from DTA measurement. In addition, the average grain diameters for the XW-42 steel subjected to the remelting temperature of 1300 and 1340 °C are about 49 ± 11 and 51 ± 10 μm, respectively.

In comparison, the structures with near-spheroidal grains are observed for AISI M2 samples as soon as most of the carbides dissolved between 1240 and 1280 °C (Fig. 9b). This temperature corresponds to 11% liquid percent according to liquid percent profile from DTA measurement. At higher temperatures of 1340 and 1360 °C, more spheroidal structures are achieved. The liquid percent that corresponds to 1340 and 1360 °C for AISI M2 samples according to DTA are 20 and 35%, respectively. The average grain sizes for these AISI M2 samples are 36 ± 3 and 42 ± 6 μm for partial remelting temperatures of 1340 and 1360 °C, respectively. The grain size found for both samples are relatively small compare to the one that is found in other steel with small amount of eutectic carbide (i.e. HP 9430 [10, 11]) due to carbide pinning effect [21]. It was observed that the biggest pinning effect was given by vanadium rich carbide/MC type carbide [20]. This explains the smaller average grains diameters detected in AISI M2 samples.

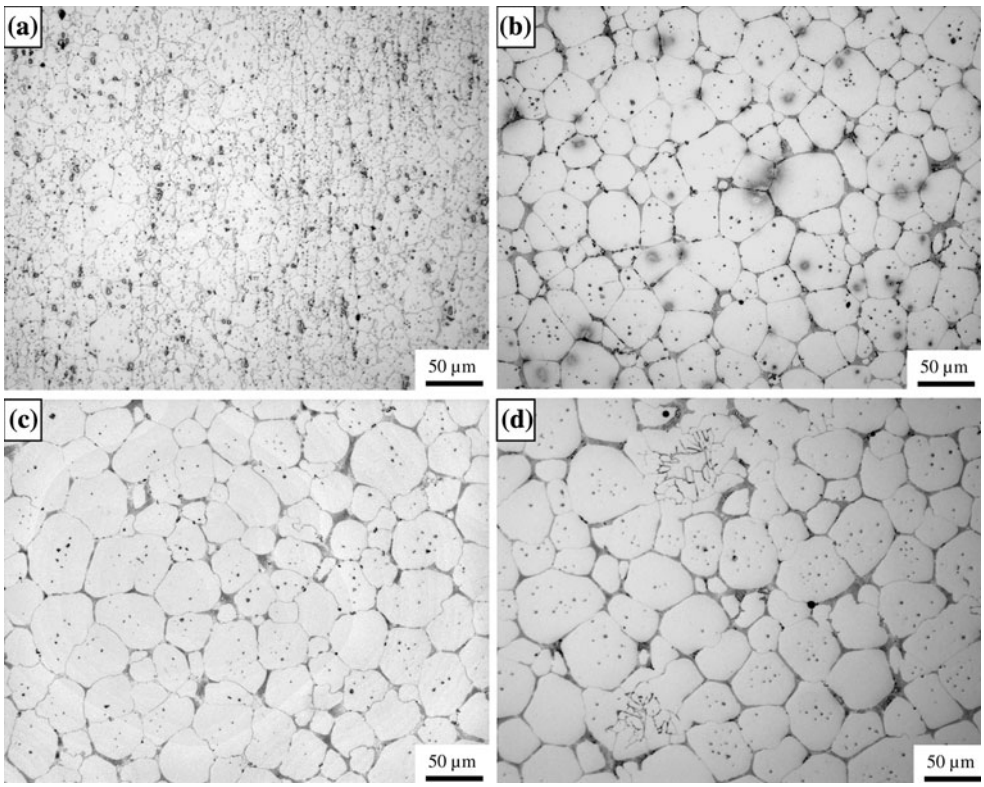

Fig. 9 Optical micrographs of AISI M2 steel after being partial remelted at **a** 1240 °C, **b** 1280 °C, **c** 1340 °C and **d** 1360 °C with 4 min holding time

The dark phase seen in Figs. 8b–d and 9b–d is liquid phase that was transformed into pearlite-like lamella structure during the quenching process. The lamella structure is due to a eutectic transformation and occurs when cementite in pearlite is replaced by other type of carbide due to the existence of alloying elements in certain critical concentration [26]. In this case, cementite was replaced by variants of MC-M_6C carbides for AISI M2 steel and M_7C_3 carbides for XW-42 steel. However, their morphology (as seen at Figs. 10 and 11) and composition (as seen at Tables 3 and 4) are different from the one that was observed in the as-received samples.

It is apparent that process of the microstructure evolutions for the two steels is similar. The transformation from equiaxed grains into near-spheroidal grains is assisted by the carbide dissolution process. Previous research [23] observed that the eutectic carbide in medium–high alloyed steels dissolved into eutectic liquid. Then, the liquid may penetrated grain boundaries when

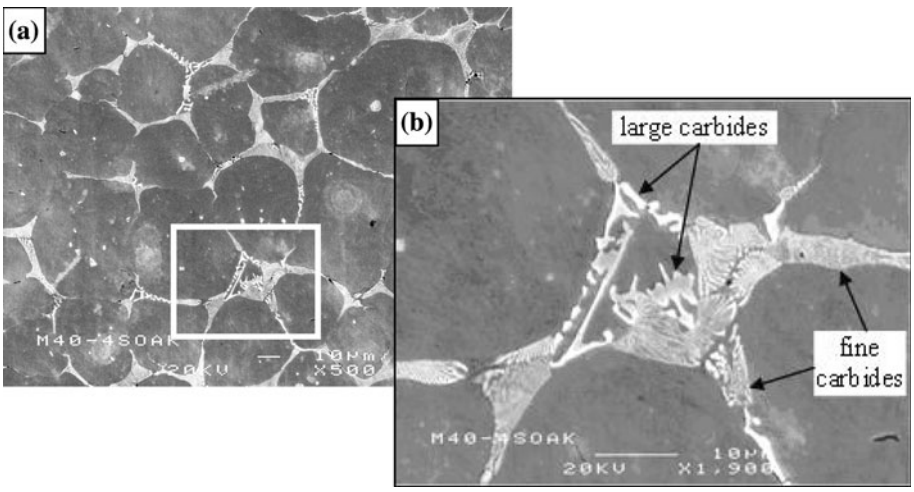

Fig. 10 SEM micrograph of quenched liquid from AISI M2 steel sample after being partial remelted at 1340 °C. **b** is the area within the *white rectangle* shown on (**a**)

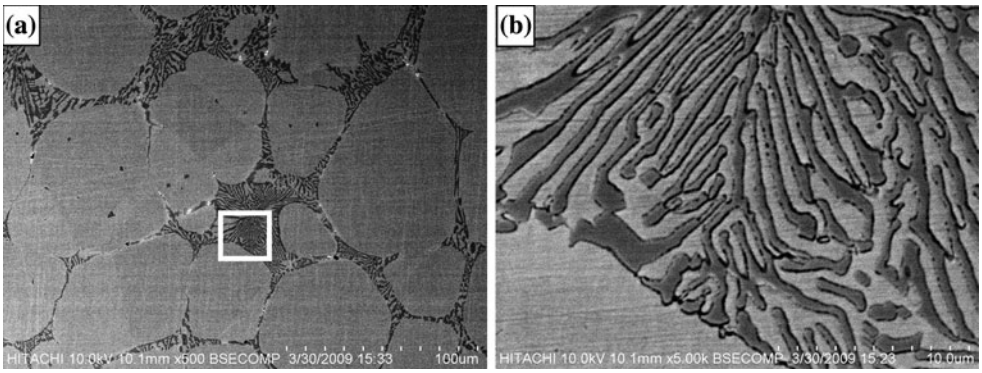

Fig. 11 SEM micrographs of quenched liquid from XW-42 steel sample after being partial remelted at 1340 °C. **b** is the area within the *white rectangle* shown in (**a**)

Table 3 EDX analysis results of the carbides found in the quenched liquid shown in Fig. 10

	Wt%					
	W	Mo	Cr	V	Fe	Co
Large carbides (MC)	19.4	18.4	4.9	28.1	28.9	0.4
	20.0	18.6	5.2	31.1	24.6	0.5
	19.2	17.5	4.8	23.9	34.9	–
Fine web-like carbides (M_6C)	12.1	13.7	6.4	4.0	63.3	0.4
	13.1	14.1	6.7	3.8	61.7	0.4
	13.2	13.8	6.6	4.1	61.5	0.5

Table 4 EDX analysis results of the fine web-like carbides found in the quenched liquid shown in Fig. 11

Wt%			
V	Cr	Fe	Mo
3.0	33.9	52.7	2.5
3.5	39.2	46.2	2.2
3.9	40.9	45.0	1.0

$$\gamma_{GB} > 2\gamma_{SL} \quad (2)$$

where γ_{SL} is the solid–liquid surface energy and γ_{GB} is the local grain boundary energy. Both are influenced by grain orientation and misorientation between grains [27]. Subsequently, melting at the sharp asperities of the equiaxed grains and solidification in regions of negative curvature due to diffusion follows and results in near-spheroidal grains [17]. Furthermore, the solid–liquid interface due to liquid penetration is necessary to provide lubrication between grains during thixotropic forming processes.

On the other hand, solid–solid interfaces between grains are also observed beside the solid–liquid interface. The solid–solid interfaces consisted of unpenetrated grain boundaries as shown by the grains with solid–solid contact zones form solid skeleton in which all grains are either connected directly (i.e. grains connected to the next neighbouring grains) or indirectly (i.e. grains connected to neighbouring grains via other grains) [28]. The solid skeleton can be observed in more detail by using a 3D model. For this purpose, a sample of XW-42 steel heated to 1340 °C for 5 min was selected for modelling by using AutoCAD software. The area that was used for modelling is the one within the black rectangle as shown in Fig. 8d. The overall 3D modelling result can be seen in Fig. 12a. A detailed examination to the model (Fig. 12b, c) found that some of the grains and/or agglomerates seen separated in 2D observation are actually connected into the solid skeleton (or a large single agglomerate, in other words). For example, agglomerate *a* in Fig. 8d which seems to be separated from its neighbours (i.e. *b*, *c*, *d*) is found to be actually connected through series of "bridges" (i.e. overlapping areas between agglomerates and or grains—marked black in Fig. 12c) directly (to grain *c*) and also indirectly (to agglomerates *b* and *d* through grain *c*) (Fig. 12c). As comparison, Fig. 13 shows the top view of the structure in a 3D wireframe prior to rendering (creating a photorealistic or realistically shaded image from a 3D wireframe/solid objects). In this angle, the bridges can be viewed clearly. A similar structure would be expected for AISI M2 steel.

The solid skeleton is useful to support the sample and prevent it from collapsing prior to forming process. However, the skeleton must also be weak enough to be deformed easily. The balance between both conditions is paramount to ensure the alloy's thixotropic property at the processing temperature.

One way to show the thixotropic behaviour of a semi-solid alloy slurry is by observing its viscosity-shear rate relationships during deformation. Figure 14 shows these relationships for AISI M2 steel when forming was carried out at 1340 and 1360 °C. For the discussion on how the graphs were produced, please refer to refs. [17, 29]. The graphs show that the viscosity decreases with increasing shear rate, indicating thixotropic behaviour at both processing temperatures. A

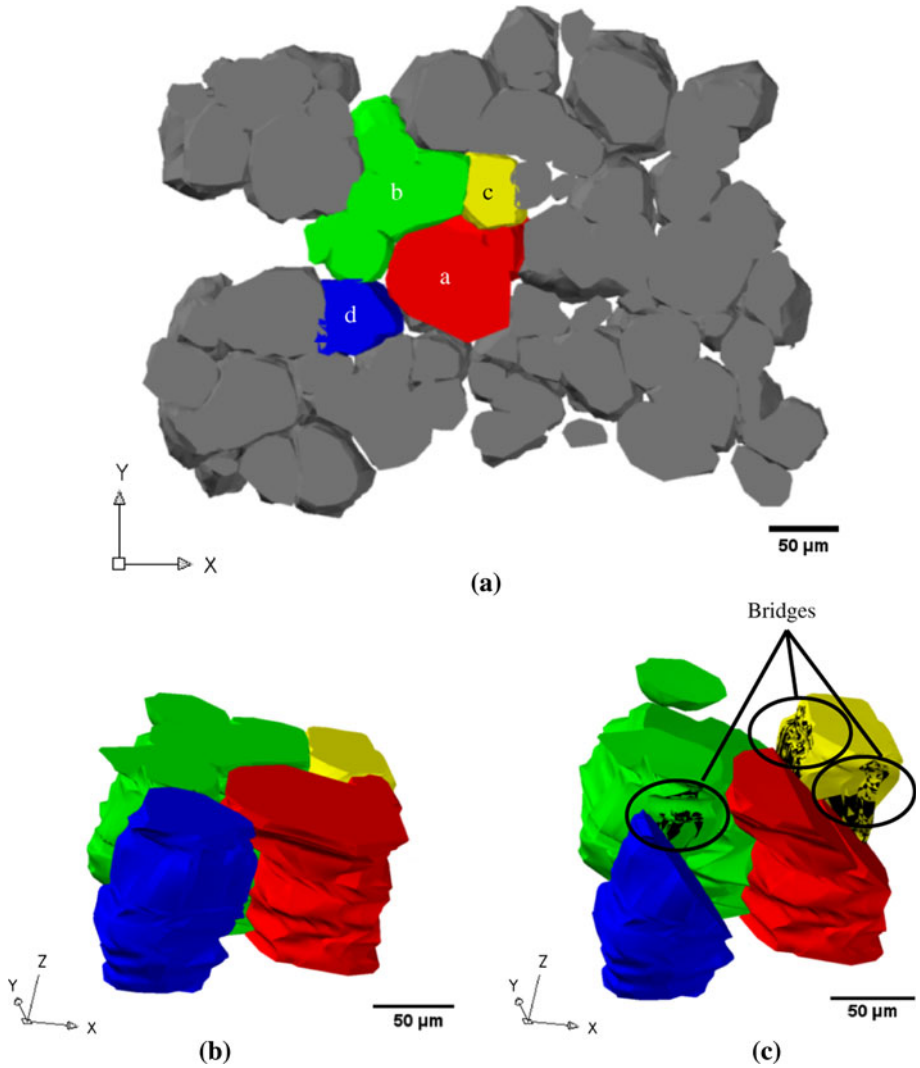

Fig. 12 **a** A 3D model of the area within the *black rectangle* shown in Fig. 8d, **b** the enlargement of the studied agglomerate (*a*,*b*,*c* and *d*) in (**a**), and **c** the sliced version of (**b**) to show "bridges" that connect agglomerate *a* and its surrounding agglomerates or grains into the solid skeleton

detail interpretation of these curves on the aspect of pseudo-plasticity can be found in Ref. [30].

Based on the above discussion, it is apparent that the direct partial remelting of these ferrous alloys from as-annealed condition successfully produces near-spheroidal grains in a liquid matrix. However, the degree of success in producing this structure depends on the steel's chemical composition. Medium to high alloyed steels such as XW-42 and AISI M2 that are rich in carbide-forming elements are more likely to successfully produce the desired structure compared to plain carbon or low alloy steels due to the role of eutectic carbides in producing near-spheroidal grains at the semi-solid temperature interval.

Conclusion

The microstructural evolution of XW-42 and AISI M2 steels after direct partial remelting from the as-annealed condition has been analysed. The as-received samples for both steels show arrays of carbides distributed in bands parallel to the working direction. The carbide bands are still clearly observed at sub-solidus temperature for both steels. In the semi-solid zone, the carbides are observed to be fully dissolved at certain temperature ranges, between 1250 and 1270 °C for XW-42 steel and between 1280 and 1300 °C for AISI M2 steel. The carbides dissolve into the liquid phase and penetrated the grain boundaries if the balance of interfacial energy is favourable. This has then resulted in the formation of near-spheroidal grains surrounded by liquid matrix. Beside solid–liquid particle contact, solid–solid interfaces were also observed for both steels in 2D as well as in 3D observations. The solid–solid interface consisted of non-penetrated grain boundary and it is useful to provide the solid skeleton to support the sample and prevent it from collapsing prior to the forming process. However, the skeleton must also be weak enough for the sample to be thixotropically deformed.

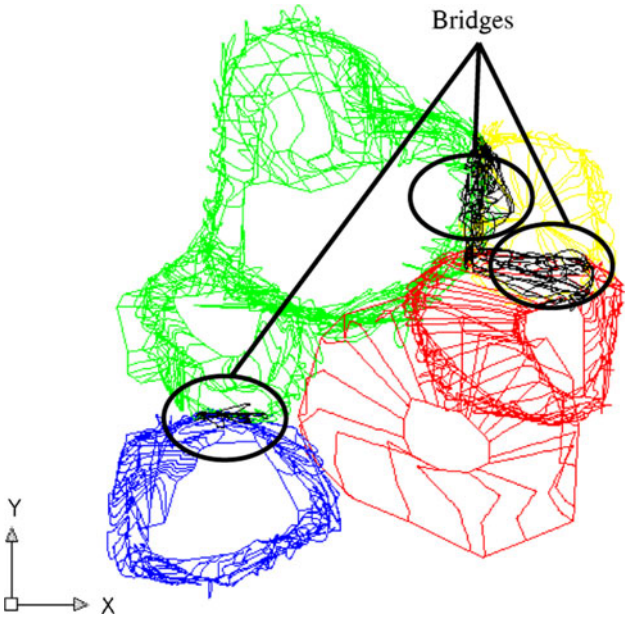

Fig. 13 Top view of the "bridges" shown in the form of 3D wireframe

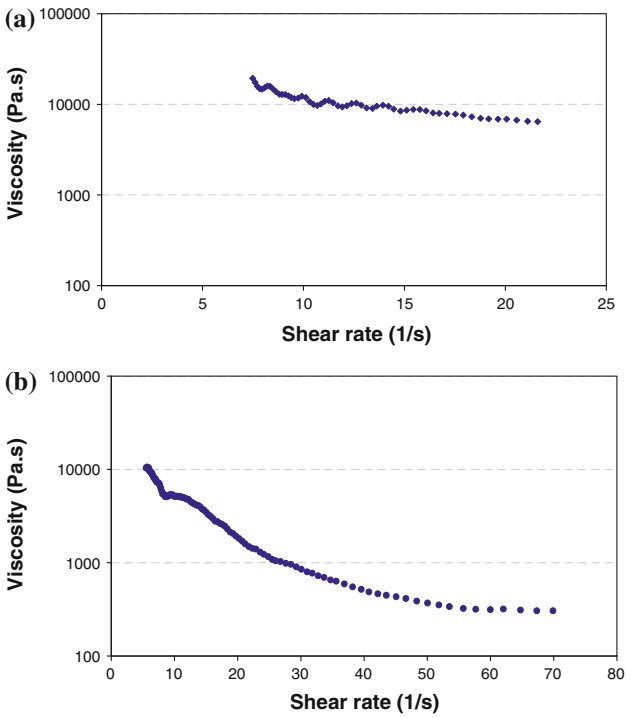

Fig. 14 Viscosity–shear rate relationships for AISI M2 sample at **a** 1340 °C and **b** 1360 °C

Acknowledgement The authors would like to thank to the Ministry of Science, Technology and Innovation (MOSTI) Malaysia for sponsoring this study and P. Kapranos of The University of Sheffield for helpful discussions.

References

1. Kapranos P, Kirkwood DH, Sellars CM (1989) In : Exner HE Schumacher V (eds) Advanced material and process, vol 1: advanced processing and high temperature materials. Proceedings EUROMAT Conference, Deutsche Gesellschaft für Metallkunde, Oberusel
2. Spencer DB, Mehrabian R, Flemings MC (1972) Metall Trans 3:1925
3. Fan Z (2002) Int Mater Rev 47:49
4. Hirt G, Khizhnyakova L, Baadjou R, Knauf F, Kopp R (2009) In: Hirt G, Kopp R (eds) Thixoforming-semi-solid metal processing. Wiley-VCH Verlag GmbH, Weinheim
5. Kirkwood DH, Suéry M, Kapranos P, Atkinson HV, Young K (2010) Semi-solid processing of alloys. Springer-Verlag, Heidelberg
6. Behrens B, Haller B, Fischer D (2004) Steel Res Int 75:561
7. Kopp R, Shimahara H, Schneider JM, Kurapov D, Telle R, Münstermann S (2004) Steel Res Int 75:569
8. Kurapov D, Scheneider JM (2004) Steel Res Int 75:577
9. Küthe F, Schonbohm A, Abel D, Kopp R (2004) Steel Res Int 75:593
10. Omar MZ, Palmiere EJ, Howe AA, Atkinson HV, Kapranos P (2005) Mater Sci Eng A395:53
11. Omar MZ, Atkinson HV, Palmiere EJ, Howe AA, Kapranos P (2004) Steel Res Int 75:552
12. Bramann H, Afrath C, Grimmig T, Fehlbier M, Bührig-Polaczek A (2004) Steel Res Int 75:537
13. Uhlenhaut DI, Kradolfer J, Püttgen W, Löffler JF, Uggowitzer PJ (2006) Acta Mater 54:2727
14. Püttgen W, Hallstedt B, Bleck W, Löffler F, Uggowitzer PJ (2007) Acta Mater 55:1033
15. Li JY, Sugiyama S, Yanagimoto J (2005) J Mater Process Technol 161:396
16. Püttgen W, Hallstedt B, Bleck W, Löffler JF, Uggowitzer PJ (2007) Acta Mater 55:6553
17. Omar MZ, Atkinson HV, Howe AA, Palmiere EJ, Kapranos P, Ghazali MJ (2009) J Mater Sci 44:869. doi:10.1007/s10853-008-3181-1
18. Kirkwood DH (1994) Int Mater Rev 39:173
19. Saunders N, Guo Z, Li X, Miodownik AP, Schillé J (2003) JOM 12:60
20. Niroumand B, Xia K (2000) Mater Sci Eng A 283:70
21. Roberts GA, Hamaker JC, Johnson AR (1971) Tool steels, 2nd edn. American Society for Metals, Metals Park
22. ASM (1998) Metals handbook, 9th edn, vol 1. ASM International, Metals Park
23. Meuser H, Bleck W (2001) Steel Res Int 72:271
24. Püttgen W, Bleck W (2004) Steel Res Int 75:531
25. Liu D, Atkinson HV, Jones H (2005) Acta Mater 53:3807
26. Bhadeshia HKDH, Honeycombe RWK (2006) Steels-microstructures and properties, 3rd edn. Butterworth-Heinemann, Oxford
27. Tzimas E, Zavaliangos A (2000) Mater Sci Eng A 289:228
28. Wolfsdorf TL, Bender WH, Voorhees PW (1997) Acta Mater 45:2279
29. Omar MZ, Palmiere EJ, Howe AA, Atkinson HV, Kapranos P (2004) In: Proceeding of the 8th international conference on semi-solid processings of alloys and composites, Limassol. North American Die Casting Association, Wheeling
30. Omar MZ, Atkinson HV, Kapranos P (2011) Metall Mater Trans A. doi:10.1007/s11661-011-0671-6